SCIENCE CHINA
Physics, Mechanics & Astronomy

•Article•

October 2022 Vol. 65 No. 10: 106111
https://doi.org/10.1007/s11433-022-1953-x

Aging and rejuvenation during high-temperature deformation in a metallic glass

Langting Zhang[1], Yunjiang Wang[2,3], Yong Yang[4,5], and Jichao Qiao[1,6*]

[1] *School of Mechanics, Civil Engineering and Architecture, Northwestern Polytechnical University (NPU), Xi'an 710072, China;*
[2] *State Key Laboratory of Nonlinear Mechanics, Institute of Mechanics, Chinese Academy of Sciences, Beijing 100190, China;*
[3] *School of Engineering Science, University of Chinese Academy of Sciences, Beijing 100049, China;*
[4] *Department of Mechanical Engineering, College of Engineering, City University of Hong Kong, Hong Kong 999077, China;*
[5] *Department of Materials Science and Engineering, College of Engineering, City University of Hong Kong, Hong Kong 999077, China;*
[6] *Innovation Center, NPU-Chongqing, Chongqing 401135, China*

Received May 21, 2022; accepted July 8, 2022; published online September 1, 2022

High-temperature deformation has been demonstrated as an effective measure to rejuvenate and optimize the mechanical properties of metallic glasses (MGs). Clarifying the competition between aging and rejuvenation during high-temperature deformation is helpful in rejuvenating MGs accurately. Signatures of aging and rejuvenation in a $La_{30}Ce_{30}Ni_{10}Al_{20}Co_{10}$ MG were investigated via high-temperature deformation and mechanical relaxation. The coupling of thermal history, aging, and mechanical disordering determines the transient deformation and the structural state of MGs. The stress overshoot and anelastic deformation induce structural rejuvenation, increasing the concentration of defects and erasing thermal history. Therefore, the eventually steady-state condition is dependent on ambient temperature and strain rate instead of the initial structure. Furthermore, the one-to-one relationship between defect concentration and strain rate clarifies the structural nature of rejuvenation in amorphous materials. Such a relationship also contributes toward a comprehensive understanding of the structural rejuvenation behavior in amorphous materials.

metallic glass, aging, rejuvenation, homogenous flow, free volume

PACS number(s): 61.43.Dq, 62.40.+i, 62.20.Hg

Citation: L. Zhang, Y. Wang, Y. Yang, and J. Qiao, Aging and rejuvenation during high-temperature deformation in a metallic glass, Sci. China-Phys. Mech. Astron. **65**, 106111 (2022), https://doi.org/10.1007/s11433-022-1953-x

1 Introduction

The properties of any type of metallic glasses (MGs) of a given composition have long been recognized to vary unpredictably, showing a detectable dependence on the microstructure tailored by the production technological parameters and subsequent treatments [1-3]. MGs have captured the attention of condensed matter physics and materials science because of their excellent mechanical and functional properties, such as excellent strength, impressively large elastic strain, and high fracture toughness [1,4-9]. Unfortunately, aging-induced structural relaxation prompts severe embrittlement and becomes a bottleneck for their engineering applications as structural materials. Consequently, this phenomenon inspires research interests in the rejuvenation of MGs, a reverse process to structural relaxation [10-12]. As a promising rejuvenation strategy, high-temperature deformation has been widely used to reverse the aging propensity and promote the thermodynamic state of MGs [12]. Tong et al. [13] reported the recovery of lost

*Corresponding author (email: qjczy@nwpu.edu.cn)

plasticity due to structural relaxation in a brittle MG by high-temperature deformation. However, deformation can also induce a relaxed state in MGs in some cases [14]. Therefore, identifying the direction of aging/rejuvenation to rejuvenate MGs accurately via high-temperature deformation urgently needs in-depth studies.

Free volume is the pivotal concept for quantifying glassy properties and phenomena, such as glass transition [13], deformation [15], and diffusion [16]. Physical aging below the glass transition temperature T_g can generally reduce the free volume content, while rejuvenation leads to an increase in such content [10,17-20]. Physical aging is different from structural relaxation. The former corresponds to spontaneous relaxation of glass toward a low energy state, while the latter relates to forced relaxation of glasses subject to a designed thermal protocol [7,8]. Despite the considerable amount of research on the rejuvenation of MGs, a quantitative description of the key factors that tailor the level of aging/rejuvenation is still lacking. The existence of a mechanical/thermal relaxation to rejuvenation transition has been recently argued [21-23]. Such an argument leads to intriguing questions: how does aging compete with rejuvenation and their correlation with free volume during the deformation? These questions will be answered by revealing the role of aging and rejuvenation upon deformation and the mechanical properties of MGs.

The degree of the structural state of MGs can generally be characterized by the value of structural enthalpy below T_g, mechanical relaxation intensity, effective disorder temperature, and some other structural indexes [24,25]. A key aspect of the current work lies in the control of the initial structural state of an MG by pre-aging before high-temperature deformation, which elucidates the deformation signatures. Tension, stress relaxation, creep, and mechanical relaxation were conducted to characterize the relaxation or rejuvenation of the sample induced by high-temperature deformation. The properties of MGs are determined by the competition between aging and rejuvenation, which is rationalized by the temporal evolution of the concentration of flow defects. The eventual dynamic equilibrium concentration is controlled by ambient temperature and the steady-state flow rate. Detailed quantitative numerical calculations reveal a significant transition from structural relaxation to rejuvenation, which promotes an understanding of rejuvenation in MGs.

2 Experimental procedure

2.1 Sample preparation

A model alloy of composition $La_{30}Ce_{30}Ni_{10}Al_{20}Co_{10}$ (at.%) was prepared by arc-melting pure metals in the argon atmosphere. The titanium getter was performed to scavenge oxidation during this process. The master alloy was remelted six times to ensure chemical homogeneity. Ribbons with a width of 1.2 mm and a thickness of 30 μm were prepared for this investigation using the single-roller melt-spinning technique.

2.2 Deformation experiments

The tensile tests were performed at 423 K below T_g (−438 K) by the tension film configuration of the commercial dynamic mechanical analyzer (DMA, TA Q800). The tensile temperature was maintained for 10 min to ensure thermal equilibration before the tensile tests, and the strain rate was chosen as 1×10^{-4} s^{-1}. A tensile load of 0.01 N was applied to reduce the bending of ribbons during the heating process. The samples had been pre-aged at 423 K several times (from 0 to 3000 s) to study the effect of physical aging on deformation.

The deformation-relaxation experiments were measured under strain rate tension with strain magnitude ranging from 0.6% to 13%.

The creep experiments were performed in tensile mode at 403 K, and the applied stress was 100 MPa. The samples had also been pre-aged at 403 K several times (from 0 to 3000 s) to study the effect of physical aging on the creep mechanism.

2.3 Dynamic mechanical relaxation experiments

The complex modulus of the glassy material is expressed as $E = \sigma/\varepsilon = E' + iE''$. E' is the storage modulus, which corresponds to the elastic response. E'' is the loss modulus, which is closely associated with the viscoelastic response. Under the simulation of a periodic stress $\sigma = \sigma_0\cos(2\pi ft)$, the strain response of MGs is monitored as $\varepsilon = \varepsilon_0\cos(2\pi ft + \delta)$, where f is the driving frequency and δ is the phase lag. The complex modulus is expressed as $E = \sigma/\varepsilon = E' + iE''$. The loss factor $\tan\delta = E''/E'$ can be determined.

3 Results and discussion

In the framework of free volume proposed by Cohen and Turnbull [26] and expanded by Spaepen [27], the flow of MGs occurs on the basis of the mobility of free volume. Free volume is defined as the "freezing in" of excess volume when melting liquids fall out of equilibrium. The plastic flow is ascribed to the activation of flow defects, which is associated with the atomic jump in nearby local holes with a size larger than the critical value. In this approach, atom jumps introduce local shears and macroscopic flow. The correlation between the flow defect concentration c_f and free volume is described as [27]:

$$c_f = \exp\left(-\frac{\gamma v^*}{v_f(T)}\right), \quad (1)$$

where γ is the geometrical factor ($0.5 < \gamma < 1$), v^* is the critical value of the hole size for atomic jump, and $v_f(T)$ is the mean free volume based on the ambient temperature. The defect concentration c_f is sensitive to the variation in free volume concentration. In other words, c_f is also dependent on the potential energy of an MG, that is, the decrease in c_f due to structural relaxation and the increase due to rejuvenation. The annihilation of c_f during structural relaxation can generally be effectively described by [27]

$$\dot{c}_f^- = -k_r c_f (c_f - c_{f,eq}), \tag{2}$$

where $\dot{c}_f^-$ is the annihilation rate of defects, k_r is an annihilation rate constant, and $c_{f,eq}$ is the temperature-dependent equilibrium concentration. The deformation is widely accepted to induce the creation of defects, and a linear correlation exists between the increments dc_f and $d\varepsilon$ (ε is the strain). de Hey et al. [28] proposed the creation rate of defects, which follows the form

$$\dot{c}_f^+ = a_x \dot{\varepsilon} c_f \ln^2(c_f), \tag{3}$$

where $\dot{c}_f^+$ is the creation rate of defects and a_x is the proportionality factor. Through eqs. (2) and (3), the evolution of c_f can be estimated as the sum of the annihilation and creation of flow defects as:

$$\dot{c}_f = \dot{c}_f^- + \dot{c}_f^+ = -k_r c_f (c_f - c_{f,eq}) + a_x \dot{\varepsilon} c_f \ln^2(c_f). \tag{4}$$

In this case, the steady-state flow stress corresponds to the dynamic balance between the annihilation and creation of flow defects ($\dot{c}_f = 0$). The dynamic equilibrium concentration c_f^* is given as:

$$c_f^* = c_{f,eq} + \frac{a_x}{k_r} \dot{\varepsilon} \ln^2(c_f). \tag{5}$$

Notably, $c_{f,eq}$ only depends on ambient temperature, but c_f^* shows a strong dependence on temperature and applied stress-strain rate. Therefore, the plastic flow of MGs is suggested to be linked to the stress-assisted, thermally activated diffusion of atoms [27]. This phenomenon leads to a relation between the flow stress and the plastic strain rate given by [27]

$$\dot{\varepsilon} = \dot{\varepsilon}_f \sinh\left(\frac{\sigma V}{2\sqrt{3} k_B T}\right), \tag{6}$$

where V is the characteristic activation volume and $\dot{\varepsilon}_f$ is the temperature-dependent strain rate factor.

Figure 1(a) shows the tensile tests of the La-based MG at various aging times. With the application of deformation, the initial stress shows an almost purely elastic response with a sublinear increase due to the existence of viscous contribution. A stress overshoot was observed when the strain reached a value of approximately 3%, which finally decayed toward a steady-state plateau at large strains (ε > 10%). Homogeneous flow can occur for MGs in the structural transience accompanying the balanced condition of free volume. This condition is observed upon strain initiation from considerably relaxed states. Strong stress overshoot is found in the aged samples. Elastic and plastic deformations occur upon loading and lead to structural evolution (accumulation of free volume) accompanied by strain softening. Consequently, the stress-strain curve displays a peak following a decrease in stress with further strain. The stress softening continues until the rate of free volume creation matches that of annihilation, that is, an eventual steady-state condition. Only one unique steady-state structure is available for any set of test conditions (i.e., temperature, stress, and strain rate). The transient in the mechanical response corresponds to the evolution of structure toward the steady state.

Aging mainly manifests in the stress overshoot peak, while the final steady-state stress is independent of aging. The independence of aging in steady-state stress indicates a unique state wherein the thermal history introduced by aging has been erased by the mechanical flow. The stress-strain curves were simulated by eqs. (4) and (6), respectively, to understand the details regarding the activation process of flow defects. The initial defect concentration $c_{f,0}$ was estimated at 8.5×10^{-14}, and the activation volume was taken as 0.25 nm^3 for the as-cast state based on a previous study [29]. The free parameters $\dot{\varepsilon}_f$, k_r, and a_x were adjusted to fit the experimental data. Figure 1(a) shows that the free volume model fits the experimental data fairly well. Bletry et al. [30] suggested that a_x/k_r and $\dot{\varepsilon}_f$ are positively and negatively related with $c_{f,eq}$, respectively, suggesting that the relative change in defect concentration $(c_f - c_{f,eq})/c_{f,eq}$ under thermal and mechanical stimulations should be examined. Figure 1(b) illustrates the evolution of $(c_f - c_{f,eq})/c_{f,eq}$ during tension. Significantly, the initial defect concentration decreases with aging time, while dynamic equilibrium concentration c_f^* is independent of aging. In addition, the stress overshoot is imperceptible if $c_{f,0}$ is equal to c_f^* [31]. Herein, a comprehensive understanding of the stress overshoot (even stress undershoot) should be provided. In the case of $c_{f,0} < c_f^*$, the flow introduces an increase in c_f, which is a rejuvenating process corresponding to the stress overshoot; if $c_{f,0} > c_f^*$, then a decrease in c_f, which is an aging process corresponding to the stress undershoot, is observed. Overall, the stress overshoot-undershoot is a product of the matching between $c_{f,0}$ and c_f^*. Net structural relaxation is observed in pre-aging samples despite the removal of the thermal history by steady-state flow because the dynamic equilibrium concentration is still smaller than the initial defect concentration of as-cast state. If optimized (in terms of strain rate and temperature), then homogenous flow holds a substantial and largely unexplored potential for achieving global rejuvena-

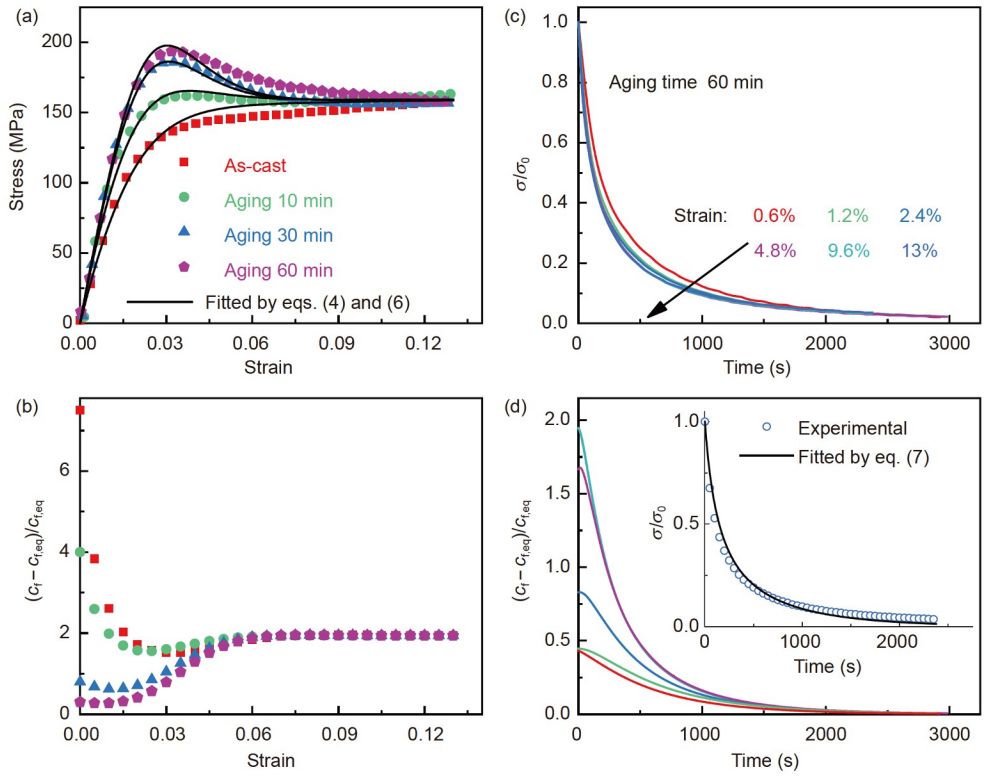

Figure 1 (Color online) (a) Stress-strain curves after various aging times. The solid lines are fitted by the free volume model. (b) Evolution of $(c_f - c_{f,eq})/c_{f,eq}$ with strain at various aging times. (c) Stress relaxation and (d) its corresponding relative change in defect concentration curves after flow cessation measured at different initial strain magnitudes ranging from 0.6% to 13%. The inset of Figure 1(d) shows a typical fitting of the stress relaxation curve.

tion in MGs.

An intriguing question has been naturally raised: how does stress-induced disordering govern the structure-property relation of MGs? This phenomenon must be related to the atomic rearrangements during homogenous flow. This point will be clarified by examination of the internal stress relaxation underlying the homogenous flow. The stress relaxation after flow cessation from elastic regime to steady-state condition during tensile measurements was examined. The stress decay is normalized by its value at flow interruption, as shown in Figure 1(c). The flow defects move fast under strain accumulation, thus relaxing the internal stress substantially fast before dynamical arrest. This condition is similar to the case of flow cessation after steady shear, wherein fast and strong stress decays are observed after flow cessation at high strain rates [32]. The samples with a low defect concentration generally retain additional internal stresses during the stress relaxation. The structural relaxation of MGs increases the relaxation time and strengthens the capacity of energy storage, as shown by the enhancement of the stress overshoot intensity in Figure 1(a). The effect of structural relaxation on stress relaxation reduces with strain, indicating a gradually structural rejuvenation. The aging effects diminish upon the realization of a full flow rejuvenation. The sample then translates into the unique steady-state structure, as demonstrated by the overlapping of stress relaxation curves with initial strains of 9.6% and 13% in Figure 1(c).

Only annihilation of flow defects occurs during stress relaxation; thus, eqs. (4) and (6) are reformulated as follows:

$$\begin{cases} \dot{c}_f = \dot{c}_f^{-} = -k_r c_f (c_f - c_{f,eq}), \\ \dot{\varepsilon} = 0. \end{cases} \tag{7}$$

The stress relaxation curves were fitted by eq. (7) to study the evolution of defect concentration. The inset of Figure 1(d) shows a typical fitting. The relative change in defect concentration $(c_f - c_{f,eq})/c_{f,eq}$ *versus* the time at various flow cessations is displayed in Figure 1(d). The significant acceleration of stress decay with defect concentration can be observed, demonstrating the close correlation of defect concentration to the mechanical properties of MGs (i.e., a glass with high defect concentration looks similar to a liquid). The dependence on defect concentration highlights the non-equilibrium nature of the glassy state attained after imposing zero-flow conditions: different structural states exist with the same thermodynamically controlling parameters but different history-dependent frozen-in properties.

A transition from a fast to a slow activation process was reported by Jiao et al. [33]. The former is related to the stochastic activation of flow defects, and the latter is associated with the cooperative motion of these defects. The

critical crossover time of the power-law relation between stress rate and time is suggested to be the signal of the onset of plastic deformation. Figure 3(a) exhibits the log-log plot of $\frac{\dot{\sigma}}{\sigma_0}$ *versus* t in stress relaxation performed after an aging time of 60 min and a flow cessation of ε~4.8%. Notably, the stress relaxation process displays a double-step power-law decay as $\frac{\dot{\sigma}}{\sigma_0} \sim t^{-\gamma_i}$, $i = 1, 2$. The intersection of the two fitting lines is defined as the crossover time τ_c. The power exponents can be readily computed as $\gamma_1 = 0.72$ and $\gamma_2 = 1.02$, with $\tau_c = 93.36$ s. The double-step decay in MGs was expressed through different approaches, such as percolation dynamics [34], thermally activated process [35], or decoupling of the relaxation dynamics [36]. However, a common characteristic is that the double-step decay is attributed to different deformation mechanisms of flow defects. The power exponents and crossover times at various flow cessations are shown in Figure 2(b) to study the evolution of double-step decay on flow cessation. The power exponent γ_1 increases with the flow cessation, whereas γ_2 almost remains constant. τ_c decreases with the flow cessation, indicating that the increase in defect concentration accelerates the transition between power-law decays. The power exponent and crossover time are independent of flow cessation under steady-state flow. The effect of flow cessation on the evolution of the exponent and crossover time is remarkably similar to that of the temperature, confirming that the effects of flow cessation and temperature move in the same direction [37]. If the value of γ_2 is roughly viewed as approximately 1, then the difference between power-law exponents becomes small with the flow cessation. Thus, flow cessation enhances the rate of stress decay. Discussing the physical origin of the power-law relation evolution upon macroscopic stress decay is interesting. When the defect concentration is relatively high, the entirely random activation of reversible flow defects is responsible for a slight stress decay, corresponding to a quick process. By contrast, the cooperative rearrangements of flow defects occur after an incubation time which breaks the initial structure, introducing irreversible deformation that casts a slow process. In addition, the increase in the initial defect concentration enhances the intensity of random activation of flow defects (indicated by the increase in γ_1). However, this phenomenon has negligible effects on the percolation of these activated defects, as demonstrated by the constant γ_2. The crossover reasonably occurs early if the initial concentration of defect is high.

Parallelly, a series of creep experiments at different aging times were performed to clarify the effects of aging and rejuvenation on the creep behavior of MGs. The strain evolution of the model alloy with different degrees of aging is illustrated in Figure 3(a). In all cases, the strain response to the stress comprises the following three components: (1) elastic strain ε_e, an instantaneous, linear, and fully recoverable component; (2) anelastic strain ε_a, a time-dependent component that induces a full recovery with a characteristic time; (3) visco-plastic strain ε_{vp}, a non-recoverable and time-dependent component. The identification of these components is shown in the inset of Figure 3(a). The magnitude of strain decreases with increasing aging time, demonstrating that structural relaxation suppresses creep in the material. However, the quasi-steady-state creep rate is unaffected by aging, which is consistent with the negligible effect of pre-aging on steady-state plateaus in tensile experiments (Figure 1(a)). The structural relaxation mainly suppresses the anelastic strain, suggesting that the anelastic deformation mainly determines the occurrence of aging or rejuvenation. Similar results have been reported by Tong et al. [38], who attributed the structural disordering of MGs in thermomechanical creep to the anelastic strain beyond a threshold. The calculated evolution of defect concentration during creep is shown in Figure 3(b). Interestingly, the evolution of defect concentration at various aging times is similar to that in tensile experiments (as shown in Figure 1(b)), verifying the consistency between strain rate- and stress-controlled models.

Modifications of physical properties of MGs, such as

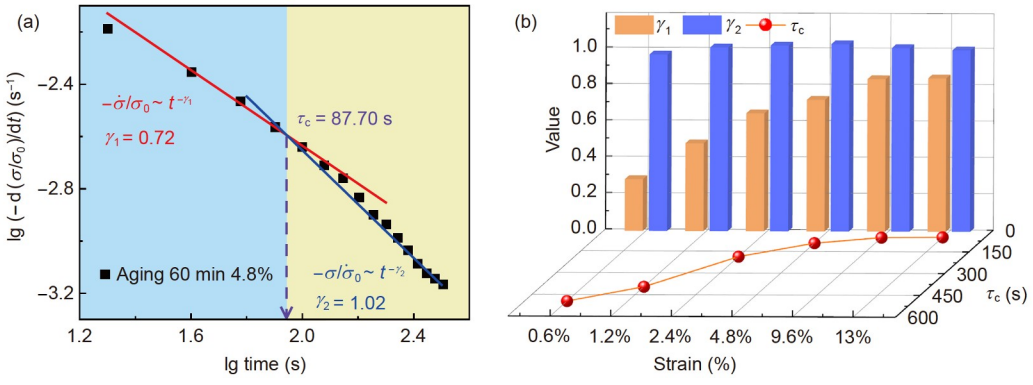

Figure 2 (Color online) (a) Log-log plot of the stress decaying rate against time at 403 K. Two relaxation regions are identified with power-law exponents of $\gamma_1 = 0.72$ and $\gamma_2 = 1.02$ corresponding to the fast and slow relaxation modes, respectively. The crossover time is $\tau_c = 93.36$ s. (b) Temperature dependence of the power-law exponents γ_1, γ_2 and the crossover time τ_c.

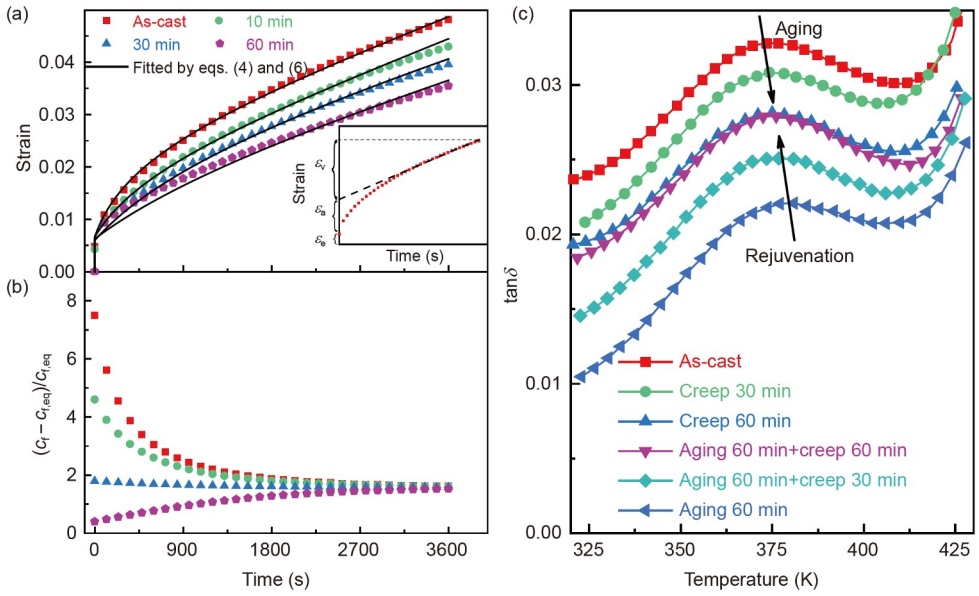

Figure 3 (Color online) (a) Creep strain and (b) its corresponding relative change of defect concentration as a function of time after flow cessation. The inset of Figure 3(a) shows the identification of elastic strain ε_e, anelastic strain ε_a, and visco-plastic strain ε_{vp}. (c) Evolution of tanδ with temperature with different thermal and mechanical histories.

modulus, density, enthalpy, and entropy, can generally be induced by various treatments. Physical aging and deformation affect atomic mobility, which can be characterized by mechanical relaxation modes based on mechanical spectroscopy. DMA is a comprehensive technique used to obtain information on the atomic movements of MGs under a sinusoidal stimulation and allows the exploration of the effect of aging and creep on mechanical relaxation. Figure 3(c) shows the evolution of the loss factor tanδ with temperature for the La-based MG at various structural states. All the curves obey an identical rule compared with that of the as-cast sample, suggesting that the structures of these samples resemble each other. The β relaxation process dominates the tanδ-T curves in all states. The principal β relaxation peaks shift to high temperature and low intensity with aging due to the annihilation of defects. In Figure 3(b), a continued decrease in the defect concentration is observed during the creep process of the as-cast sample. Consequently, a net structural relaxation is introduced to the system. For example, creep induces a continuous increase in defect concentration in the pre-aged sample for 60 min. Meanwhile, the intensity of β relaxation enhances while the peak shifts to the low-temperature region, a phenomenon indicating structural rejuvenation. The increase in loss factor is clear evidence of the enhancement in atomic mobility. This phenomenon also indicates that the microstructure of the aged sample is effectively modified. The β relaxation in MGs originated from microstructural heterogeneity, which is modeled as the heterogeneous distribution of solid- and liquid-like regions [39-41]. As previously mentioned, the activation of flow defects occurs in the loosely packed regions where the size of nearby local holes is larger than the critical value. The β relaxation of the pre-aging sample is easily improved by creep, demonstrating that the free volume created as the initial concentration is sufficiently low. The recovery of the structural heterogeneity by high-temperature creep should be considered powerful evidence for optimizations of the structural index by mechanical viscoelastic deformation. This finding is interesting because high-temperature creep is an intelligent way to tailor the energy state of MGs.

The above results suggest that the energy state of MGs depends on ambient temperature and applied stress rather than the thermal and mechanical history. Consequently, a strain rate/stress threshold should exist between aging and rejuvenation, which has been observed in previous work [38,42,43]. The construction of this aging-rejuvenation diagram based on free volume should be determined theoretically. Considering the physical explanation of the parameters in eqs. (4) and (6), the structural evolution of MGs during creep is readily obtained by numerical calculations. The creep curve of the as-cast state in Figure 3(a) was taken as the reference for further calculations. The effect of $c_{f,0}$ has been discussed above. In addition, the effect of the activation volume V, rate factor $\dot{\varepsilon}_f$, and ratio a_x/k_r on the evolution of deformation and defect concentration moves in the same direction (for simplicity, only the effect of a_x/k_r is shown herein). Figure 4(a)-(c) show the evolution of ε, $\dot{\varepsilon}$, and $(c_f - c_{f,eq})/c_{f,eq}$ with time, spanning the a_x/k_r range from 6×10^{-13} to 1.6×10^{-12}. An acceleration of the deformation can also be observed. $a_x/k_r = 1.4 \times 10^{-12}$ can be viewed as a threshold because of the quasi-constant strain rate. A vital

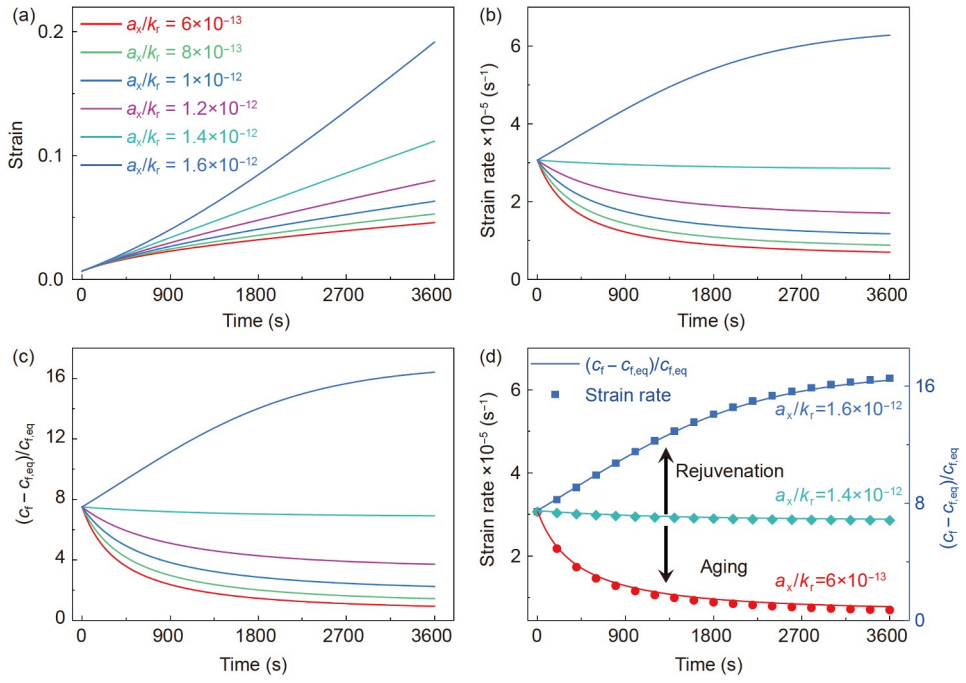

Figure 4 (Color online) Evolution of (a) ε, (b) $\dot{\varepsilon}$, and (c) $(c_f - c_{f,eq})/c_{f,eq}$ with time, spanning the a_x/k_r range from 6×10^{-13} to 1.6×10^{-12}. (d) One-to-one correlation between $\dot{\varepsilon}$ and $(c_f - c_{f,eq})/c_{f,eq}$ with different values of a_x/k_r.

point that must be clarified is as follows: k_r corresponds to the annihilation rate of flow defects while a_x determines the creation rate. The values of a_x/k_r control the orientation of structural evolution toward aging or rejuvenation. Interestingly, the evolution of $(c_f - c_{f,eq}) / c_{f,eq}$ with time is similar to that of $\dot{\varepsilon}$, as shown in Figure 4(c). At a low value of a_x/k_r, the annihilation of flow defects and the suppression of strain rates are ascribed to the net structural relaxation until the steady-state flow. A global rejuvenation trend characterized by $c_{f,0} < c_f^*$ is observed after crossing the threshold of a_x/k_r. Figure 4(d) shows the correlation between macrostructural deformation and microstructural defects, providing strong evidence of a one-to-one correlation between $\dot{\varepsilon}$ and $(c_f - c_{f,eq}) / c_{f,eq}$. The degree of the structural state of MGs (confirmed by defect concentration) depends on the ambient temperature and the steady-state flow rate. Consequently, the disagreement between steady-state flow rate and threshold rate is verified to be the trigger of structural evolution; that is, $\dot{\varepsilon} > \dot{\varepsilon}^*$ leads to rejuvenation while aging is the contrast. An acceleration of the deformation and a transition from aging to rejuvenation can be observed by optimizing the aforementioned kinetic parameters.

4 Conclusions

Overall, the aging and rejuvenation during high-temperature deformation in a MG in the framework of the free volume theory are explored. The thermal history, aging, and mechanical disordering are coupled in deformation; they cooperatively determine the deformation mechanism of MGs. Discernible differences can also be observed in the tensile experiment and creep due to aging. Moreover, the stress overshoot and anelastic deformation are closely correlated to structural rejuvenation, which erases the thermal history. The ambient temperature and the applied strain-stress rate modify the steady-state condition. Moreover, a one-to-one relationship is observed between defect concentration and strain rate creep, confirming that the competition between the creation and annihilation of flow defects is the key to opening the door of rejuvenation. The obtained findings will encourage additional work in exploring the signatures of aging and rejuvenation of MGs under some other stimuli, such as electric/magnetic fields.

This work was supported by the National Natural Science Foundation of China (NSFC) (Grant No. 51971178), the Natural Science Basic Research Plan for Distinguished Young Scholars in Shaanxi Province (Grant No. 2021JC-12), and the Natural Science Foundation of Chongqing (Grant No. cstc2020jcyj-jqX0001). The investigation of Langting Zhang is sponsored by the Innovation Foundation for Doctor Dissertation of Northwestern Polytechnical University (Grant No. CX2021015). Yunjiang Wang was financially supported by NSFC (Grant No. 12072344), and the Youth Innovation Promotion Association of the Chinese Academy of Sciences. Yong Yang acknowledges financial support from the Research Grant Council (RGC) and the Hong Kong government through the General Research Fund (GRF) (Grant Nos. CityU11200719, and CityU11213118).

1 W. Johnson, Prog. Mater. Sci. **30**, 81 (1986).
2 Y. J. Lü, C. C. Guo, H. S. Huang, J. A. Gao, H. R. Qin, and W. H. Wang, Acta Mater. **211**, 116873 (2021).

3 J. C. Qiao, L. T. Zhang, Y. Tong, G. J. Lyu, Q. Hao, and K. Tao, Adv. Mech. **52**, 117 (2022).
4 B. Sarac, and J. Eckert, Prog. Mater. Sci. **127**, 100941 (2022).
5 A. Inoue, B. Shen, H. Koshiba, H. Kato, and A. R. Yavari, Nat. Mater. **2**, 661 (2003).
6 M. M. Trexler, and N. N. Thadhani, Prog. Mater. Sci. **55**, 759 (2010).
7 D. Şopu, S. Scudino, X. L. Bian, C. Gammer, and J. Eckert, Scripta Mater. **178**, 57 (2020).
8 J. C. Qiao, Q. Wang, J. M. Pelletier, H. Kato, R. Casalini, D. Crespo, E. Pineda, Y. Yao, and Y. Yang, Prog. Mater. Sci. **104**, 250 (2019).
9 W. H. Wang, Prog. Mater. Sci. **106**, 100561 (2019).
10 W. Dmowski, Y. Yokoyama, A. Chuang, Y. Ren, M. Umemoto, K. Tsuchiya, A. Inoue, and T. Egami, Acta Mater. **58**, 429 (2010).
11 G. Ding, C. Li, A. Zaccone, W. H. Wang, H. C. Lei, F. Jiang, Z. Ling, and M. Q. Jiang, Sci. Adv. **5**, eaaw6249 (2019).
12 Y. Sun, A. Concustell, and A. L. Greer, Nat. Rev. Mater. **1**, 16039 (2016).
13 Y. Tong, W. Dmowski, Y. Yokoyama, G. Wang, P. K. Liaw, and T. Egami, Scripta Mater. **69**, 570 (2013).
14 S. Küchemann, C. Liu, E. M. Dufresne, J. Shin, and R. Maaß, Phys. Rev. B **97**, 014204 (2018).
15 J. C. Ye, J. Lu, C. T. Liu, Q. Wang, and Y. Yang, Nat. Mater. **9**, 619 (2010).
16 K. Rätzke, P. W. Hüppe, and F. Faupel, Phys. Rev. Lett. **68**, 2347 (1992).
17 A. D. Phan, A. Zaccone, V. D. Lam, and K. Wakabayashi, Phys. Rev. Lett. **126**, 025502 (2021), arXiv: 2007.15524.
18 T. J. Lei, L. R. DaCosta, M. Liu, W. H. Wang, Y. H. Sun, A. L. Greer, and M. Atzmon, Acta Mater. **164**, 165 (2019).
19 B. Ruta, E. Pineda, and Z. Evenson, J. Phys.-Condens. Matter **29**, 503002 (2017).
20 P. Lunkenheimer, R. Wehn, U. Schneider, and A. Loidl, Phys. Rev. Lett. **95**, 055702 (2005), arXiv: cond-mat/0503449.
21 K. Sun, G. Wang, Y. W. Wang, H. C. Chen, L. Yan, S. Pauly, Y. H. Wu, H. Weber, Q. Wang, B. Huang, Y. D. Jia, J. Yi, and Q. J. Zhai, Scripta Mater. **180**, 34 (2020).
22 M. Zhang, Y. M. Wang, F. X. Li, S. Q. Jiang, M. Z. Li, and L. Liu, Sci. Rep. **7**, 625 (2017).
23 Q. Sun, D. M. Miskovic, H. Kong, and M. Ferry, Appl. Surf. Sci. **546**, 149048 (2021).
24 J. Ketkaew, W. Chen, H. Wang, A. Datye, M. Fan, G. Pereira, U. D. Schwarz, Z. Liu, R. Yamada, W. Dmowski, M. D. Shattuck, C. S. O′ Hern, T. Egami, E. Bouchbinder, and J. Schroers, Nat. Commun. **9**, 3271 (2018).
25 J. Yang, Y. J. Wang, E. Ma, A. Zaccone, L. H. Dai, and M. Q. Jiang, Phys. Rev. Lett. **122**, 015501 (2019).
26 M. H. Cohen, and D. Turnbull, J. Chem. Phys. **31**, 1164 (1959).
27 F. Spaepen, Acta Metall. **25**, 407 (1977).
28 P. de Hey, J. Sietsma, and A. van den Beukel, Acta Mater. **46**, 5873 (1998).
29 L. T. Zhang, Y. J. Wang, E. Pineda, H. Kato, Y. Yang, and J. C. Qiao, Scripta Mater. **214**, 114673 (2022).
30 M. Bletry, P. Guyot, J. J. Blandin, and J. L. Soubeyroux, Acta Mater. **54**, 1257 (2006); M. Bletry, P. Guyot, Y. Brechet, J. J. Blandin, and J. L. Soubeyroux, Acta Mater. **55**, 6331 (2007).
31 Y. T. Cheng, Q. Hao, J. M. Pelletier, E. Pineda, and J. C. Qiao, Int. J. Plast. **146**, 103107 (2021).
32 M. Ballauff, J. M. Brader, S. U. Egelhaaf, M. Fuchs, J. Horbach, N. Koumakis, M. Krüger, M. Laurati, K. J. Mutch, G. Petekidis, M. Siebenbürger, T. Voigtmann, and J. Zausch, Phys. Rev. Lett. **110**, 215701 (2013), arXiv: 1302.3914.
33 W. Jiao, B. A. Sun, P. Wen, H. Y. Bai, Q. P. Kong, and W. H. Wang, Appl. Phys. Lett. **103**, 081904 (2013).
34 Y. C. Wu, B. Wang, Y. C. Hu, Z. Lu, Y. Z. Li, B. S. Shang, W. H. Wang, H. Y. Bai, and P. F. Guan, Scripta Mater. **134**, 75 (2017).
35 J. C. Qiao, Y. J. Wang, L. Z. Zhao, L. H. Dai, D. Crespo, J. M. Pelletier, L. M. Keer, and Y. Yao, Phys. Rev. B **94**, 104203 (2016).
36 P. Luo, P. Wen, H. Y. Bai, B. Ruta, and W. H. Wang, Phys. Rev. Lett. **118**, 225901 (2017), arXiv: 1609.09611.
37 L. T. Zhang, Y. J. Duan, D. Crespo, E. Pineda, Y. J. Wang, J. M. Pelletier, and J. C. Qiao, Sci. China-Phys. Mech. Astron. **64**, 296111 (2021).
38 Y. Tong, W. Dmowski, H. Bei, Y. Yokoyama, and T. Egami, Acta Mater. **148**, 384 (2018).
39 B. Cui, Z. Evenson, B. Fan, M. Z. Li, W. H. Wang, and A. Zaccone, Phys. Rev. B **98**, 144201 (2018), arXiv: 1810.02967.
40 H. B. Yu, R. Richert, and K. Samwer, Sci. Adv. **3**, e1701577 (2017).
41 K. L. Ngai, Z. Wang, X. Q. Gao, H. B. Yu, and W. H. Wang, J. Chem. Phys. **139**, 014502 (2013), arXiv: 1303.7424.
42 G. Ding, F. Jiang, X. Song, L. H. Dai, and M. Q. Jiang, Sci. China-Phys. Mech. Astron. **65**, 264613 (2022).
43 D. J. Lacks, and M. J. Osborne, Phys. Rev. Lett. **93**, 255501 (2004).